

See discussions, stats, and author profiles for this publication at: <https://www.researchgate.net/publication/264815005>

Stable Constellations of Frozen Elliptical Inclined Lunar Orbits

Article in *The Journal of the Astronautical Sciences* · July 2005

DOI: 10.1007/BF03546355

CITATIONS

85

READS

4,453

1 author:



Todd Ely

California Institute of Technology

101 PUBLICATIONS 1,522 CITATIONS

SEE PROFILE

Stable Constellations of Frozen Elliptical Inclined Lunar Orbits

Todd A. Ely¹

Abstract

Higher altitude orbits (in the 500 to 20,000 km range) at the Moon are dominated by Earth perturbations and result in motions that do not ascribe to the standard notions of orbits dominated by nonspherical gravity effects (such as from oblateness). This fact complicates orbit design of lunar orbiter constellations that require specific and persistent coverage over a selected lunar region. Using a combination of analytical theory and numerical simulation, a technique is developed for designing a lunar constellation of three spacecraft where two spacecraft are always in view from the lunar surface for the polar regions.

Introduction

A great deal of scientific interest exists regarding the permanently shadowed craters near the poles of the Moon where there may be frozen volatiles [1]. These regions, particularly the Moon's South Pole, have been proposed for extensive robotic and human exploration [2]. Unfortunately, they are typically not in view of Earth, and would require some form of communication relay to facilitate exploration via robotic and/or human missions. One solution for such a relay is a long-lived constellation of lunar telecommunication orbiters providing focused coverage at the pole of interest. Robust support requires this coverage to be continuous and redundant [3]. Finally, in order to minimize costs, this constellation should have three satellites or fewer and possess coverage properties that persist [3].

Constellation Coverage and Orbit Considerations

The combination of redundant, continuous, and focused coverage with a small number of satellites leads to the consideration of orbits with the following orbital characteristics:

1. Sufficiently large semimajor axis values to produce continuous single and double coverage with a minimal number of satellites.

¹Senior Engineer, Guidance, Navigation, and Control Section, Jet Propulsion Laboratory, California Institute of Technology, MS 301-125L, 4800 Oak Grove Drive, Pasadena, CA 91109-8099. Email: Todd.A.Ely@jpl.nasa.gov.

2. Large eccentricity values to focus coverage near apoapsis for longer contact durations.
3. Inclination values to orient the coverage swaths over the poles (rather than the equator).
4. Argument of periapsis values set to either 90° or 270° depending on whether apoapsis should be over the South Pole or North Pole, respectively.

In response to this need, a new class of stable altitude orbits at the Moon has been found that enables the presence of a constellation of lunar orbiting telecommunication spacecraft. The orbits are elliptical with their line of apsides librating in the polar region (a.k.a. "frozen" orbits), and exhibit lifetimes in excess of ten years, the expected mission duration for a lunar telecommunications system. This paper describes the processes for selecting the orbital parameters for the constellation and the mechanisms behind its subsequent stable, long-term evolution. It is also shown that, with appropriate selection of initial semimajor axis values, satellites in the same orbital plane can maintain a relatively stable mean separation between them with little or no orbit maintenance costs. That is, the constellation maintains a "formation" using only natural gravity effects and has long-term stable constellation coverage properties. Indeed, it is shown that a constellation of three spacecraft can yield continuous coverage with two spacecraft continuously in view of a polar station for the lifetime of a ten year mission.

Earth's gravity is the most significant perturbation on high altitude lunar orbits in the 500 to 20,000 km range (at higher altitudes the problem approaches a three-body problem versus a two-body perturbed problem). As a result, these orbits can possess a multitude of complex motions which are atypical of lower altitude orbits dominated by non-spherical gravity field perturbations. Indeed, many can exhibit unstable characteristics [4]. It is not uncommon for a near circular orbit to become near hyperbolic on the order of tens of days. A classic technique to minimize variations in eccentricity when nonspherical gravity zonal harmonic perturbations dominate is to utilize the J_2 and J_3 nonspherical gravity terms to design an orbit with small oscillations in eccentricity and a librating argument of periapsis (a.k.a., a "frozen orbit") [5]. This approach typically yields a solution with a small eccentricity, thus is not well suited to providing increased coverage to a selected polar region. Plus, because of the dominance of the Earth's gravity field, these solutions may not exist at higher altitudes. However, there exists another class of "frozen" orbits due to the influence of third-body perturbations (i.e. Earth gravity perturbations) that could prove useful. Ely and Howell [6] showed, in the case of Earth elliptical orbits near the critical inclination being perturbed by the Moon, that there exists a small region of stable libration motion in the $e - \omega$ phase space (e is eccentricity, and ω is the argument of periapsis) near $\omega = 90^\circ$ and 270° that is surrounded by a large region of chaotic motion. The *stable* libration motion is of particular interest, because it implies that orbits can be designed to have focused coverage at the poles. Even though the analysis was specific to the Earth, the conclusion is generic to any two-body orbit being perturbed by a third body. In the present case, that would be a lunar orbit being perturbed by the Earth. In the next section, a dynamical model with only Earth perturbations present is developed that captures the key qualitative features of the motion, and that can be used for the initial orbit design.

Initial Design Using an Earth Perturbation Long Period Model

Many authors have examined the third-body perturbation problem, some of which include Kozai [7], Lidov [8], Lorell [9], and, recently, Broucke [10] and Prado [11]. All these authors developed a simplified mean element model of an orbit being perturbed by a third body that was amenable to characterizing and classifying the essential types of the integrable motions that could exist. It should be noted that these authors did not examine the possibility that non-integrable (i.e. chaotic) motions could exist with a more complete dynamical model. Nonetheless, the models they developed prove useful for revealing the structure of the stable $e - \omega$ libration motion that can be utilized in designing the constellation.

Two reference frames relevant to the development of the model and the ensuing numerical simulations include the following:

1. A frame where the reference plane is defined by the Earth’s apparent orbit around the Moon with the x-axis of the frame defined by the intersection of Moon’s equatorial plane with the Earth’s apparent orbital plane. Note that in this frame, the Moon’s pole is inclined with respect to the Earth orbit normal at approximately $i_M^E \sim 6.8^\circ$. This frame is useful because it yields the simplest form for the mean motion model when only Earth perturbations are present. An illustration of this frame is shown in Fig. 1. The precise definition of the frame is as follows:
 - a. The standard IAU definition [12] of the Moon’s pole is defined as the normal to the Moon’s equatorial plane, and the unit vector along the pole is identified as $\hat{\mathbf{i}}_p$.
 - b. The z-axis unit vector of the frame is defined in the direction of the orbit normal of the “apparent” Earth orbit around the Moon using

$$\hat{\mathbf{z}}^{op} \equiv \frac{\mathbf{r}_E \times \mathbf{v}_E}{|\mathbf{r}_E \times \mathbf{v}_E|} \tag{1}$$

where \mathbf{r}_E and \mathbf{v}_E are the Earth’s position and velocity with respect to the Moon, respectively. The DE 405 planetary ephemerides [13] are used in the subsequent simulations to obtain values for the above vectors.

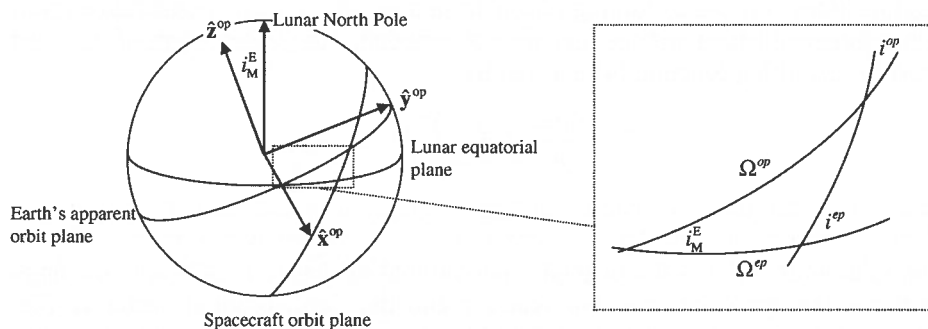


FIG. 1. The Earth Orbit Plane Frame $\{\hat{\mathbf{x}}^{op}, \hat{\mathbf{y}}^{op}, \hat{\mathbf{z}}^{op}\}$ Shown with Respect to the Lunar Equatorial Plane, and the Spherical Triangle that Relates the Spacecraft Orbit Plane, the Equatorial Plane, and the Earth Orbit Frame that Determines the Relationship in Equation (4).

c. The x-axis unit vector is defined as

$$\hat{\mathbf{x}}^{\text{op}} = \frac{\hat{\mathbf{I}}_p \times \hat{\mathbf{z}}^{\text{op}}}{|\hat{\mathbf{I}}_p \times \hat{\mathbf{z}}^{\text{op}}|} \quad (2)$$

Note that this unit vector lies along the intersection of the Earth's apparent orbit plane around the Moon and the Moon's equatorial plane.

d. Finally, the y-axis unit vector is defined by completing the triad using

$$\hat{\mathbf{y}}^{\text{op}} = \hat{\mathbf{z}}^{\text{op}} \times \hat{\mathbf{x}}^{\text{op}} \quad (3)$$

- e. Technically the Earth orbit frame "op" is not an inertial frame because of the slow variation in time of the unit vectors with respect to Earth Mean Equator frame of J2000 (EME2000). Therefore, subsequent numerical integrations may define inputs and outputs in the Earth orbit frame; however, the actual integrations take place in EME2000 to ensure an inertial integration.
2. The standard IAU Moon Pole frame [12] in which the Moon's equatorial frame is the reference plane. This is the natural frame for designing the constellation's coverage properties.

Orbital elements defined with respect to the Earth orbit plane frame are identified with the superscript "op" (short for orbit plane), and orbital elements defined with respect to the IAU Moon Pole frame are identified with the superscript "ep" (short for equatorial plane). A particular relationship that proves useful in the subsequent analysis relates the orbital inclinations defined in these two frames is

$$\cos i^{\text{op}} = \cos i_M^{\text{E}} \cos i^{\text{op}} - \sin i_M^{\text{E}} \sin i^{\text{op}} \cos \Omega^{\text{op}} \quad (4)$$

where i^{op} is the spacecraft inclination with respect to the Moon's equatorial plane, i_M^{E} is the inclination of the Earth's orbit plane with respect to the Moon's equatorial plane, i^{op} is the spacecraft inclination with respect to the Earth's orbit plane around the Moon, and Ω^{op} is the spacecraft ascending node in the Earth's orbit plane. The highlighted spherical triangle in Fig. 1 illustrates the geometry associated with equation (4). It should be noted that the orbital semimajor axis a , eccentricity e , and mean anomaly M are the same in either frame, hence are not distinguished via superscripts.

The model development begins with the construction of a disturbing function that includes only the perturbing effects from the Earth. Gravity perturbations from a nonspherical Moon and the Sun are not included. The general form of the Earth gravity disturbing function [4] is given by

$$R = \frac{Gm_E}{r_E} \sum_{l \geq 2} \left(\frac{r}{r_E} \right)^l P_l(\cos \psi_E) \quad (5)$$

where G is the universal constant of gravitation, m_E is the mass of the Earth, r_E is the distance from the Moon to the Earth, r is the distance from the Moon to the spacecraft, $P_l(\cdot)$ is the Legendre polynomial of degree l , and ψ_E is the angle between the spacecraft position vector \mathbf{r} and the Earth position vector \mathbf{r}_E (i.e., $r r_E \cos \psi_E = \mathbf{r} \cdot \mathbf{r}_E$). A simplified disturbing function that is amenable to a qualitative analysis is developed using the following assumptions:

1. Retain only the largest term in equation (5), that is $l = 2$. This is reasonable for a qualitative analysis. For example, a spacecraft at $r = 6400$ km yields the ratios

$$\left(\frac{r}{r_E}\right)^2 / \left(\frac{r}{r_E}\right)^3 \sim 60 \quad (6)$$

implying the term with $l = 3$ is 60 times smaller than the retained term.

2. Approximate the Earth's apparent orbit around the Moon as circular. This is approximately correct since the Earth's mean eccentricity is small with a value of 0.058.
3. Short period terms dependent on the spacecraft's mean anomaly M and the Earth's mean anomaly M_E are averaged out to produce a *mean element* model. Any solutions generated from the resulting model produce mean elements; to get the equivalent osculating elements requires a transformation. The impact of this transformation is noted in the numerical results presented later.

Applying the above assumptions to equation (5) produces a disturbing function of the form

$$R = \frac{\gamma n_E^2 a^2}{16\sqrt{1-e^2}} \left[(1 + 3 \cos 2i^{op}) \left(1 + \frac{3}{2} e^2 \right) + 15e^2 \sin^2 i^{op} \cos 2\omega^{op} \right] \quad (7)$$

where, as indicated previously, the orbital elements are reconciled with respect to the Earth orbit frame. The mass ratio is defined as $\gamma = \frac{m_E}{m_E + m_M}$ where m_M is the mass of the Moon and the mean motion of the Earth around the Moon is

$$n_E = \sqrt{\frac{G(m_E + m_M)}{a_E^3}}$$

The associated differential equations for secular and long period motion of $e - \omega^{op}$ are obtained by applying Lagrange's planetary equations to equation (7) with the result

$$\frac{de}{dt} = \frac{15}{8} \gamma \frac{n_E^2}{n} e \sqrt{1-e^2} \sin^2 i^{op} \sin 2\omega^{op} \quad (8)$$

$$\frac{d\omega^{op}}{dt} = \frac{3}{8\sqrt{1-e^2}} \gamma \frac{n_E^2}{n} [(5 \cos^2 i^{op} - 1 + e^2) + 5(1 - e^2 - \cos^2 i^{op}) \cos 2\omega^{op}] \quad (9)$$

Where the mean motion of the spacecraft is $n \equiv \sqrt{\frac{Gm_M}{a^3}}$. Solutions to equations (8) and (9) that are of particular interest are the stable librations of $e - \omega^{op}$ around the fixed point solutions where $e - \omega^{op}$ remain constant (i.e., $\frac{de}{dt} = \frac{d\omega^{op}}{dt} = 0$). Examination of the equations reveals the fixed point solutions when the conditions are met

$$\sin 2\omega^{op} = 0 \quad (10)$$

and

$$(5 \cos^2 i^{op} - 1 + e^2) + 5(1 - e^2 - \cos^2 i^{op}) \cos 2\omega^{op} = 0 \quad (11)$$

which leads to the results

$$\omega^{\text{op}} = 90^\circ, 270^\circ \text{ and } e^2 + \frac{5}{3} \cos^2 i^{\text{op}} = 1 \quad (12)$$

In addition to the particular fixed point solutions, equations (8) and (9) are completely integrable with the general solution

$$(1 - e^2) \cos^2 i^{\text{op}} \equiv \alpha \quad (13)$$

and

$$e^2 \left(1 - \frac{5}{2} \sin^2 i^{\text{op}} \sin^2 \omega^{\text{op}} \right) \equiv \beta = \frac{5}{2} R + \frac{15}{8} \alpha \quad (14)$$

where α is a constant of motion and is related to the z-component of the angular momentum and β is a constant of motion related to the disturbing function R (also a constant of motion) and α (c.f., the last term in equation (14)). Note that the fixed point solutions given by equation (12) are included in equations (13) and (14).

Before discussing solutions to equations (13) and (14), it is useful to discuss another class of frozen orbits that exist due to the zonal harmonics. A recent study by Elife [16] investigated families of low altitude (<500 km) frozen orbits at the Moon for zonal harmonics up to degree 20. Their results showed that for inclinations i^{op} (with respect to the equatorial plane) up to 63° there exist continuous families of frozen orbits with stable librations of $e - \omega^{\text{op}}$ for certain paired values of eccentricity and inclination. At higher inclinations there exist families of stable and unstable frozen orbits (unstable means the argument of periaapsis circulates). As noted previously, the zonal harmonics are less significant than the Earth perturbations in the current study. Nevertheless, the equatorial inclination of 63° was selected for the initial constellation design because it brings the orbital plane as close as possible to the pole, and still yields stable $e - \omega^{\text{op}}$ librations due to the zonal harmonics. As will be seen, the equivalent inclination in the Earth orbit plane i^{op} also yields stable $e - \omega^{\text{op}}$ librations from Earth perturbations.

Figure 2 illustrates some example trajectories resulting from solutions to equations (13) and (14) in the $e - \omega^{\text{op}}$ phase plane. Note that two types of trajectories for $e - \omega^{\text{op}}$ motion are illustrated: closed librations and open circulations. The paired sets of numbers shown on figure are the initial eccentricity and inclination for each trajectory; all trajectories begin with an initial argument of periaapsis value that is either 90° or 270° . The division between open or closed motions occurs when $\beta = 0$ which exists either for $e = 0$ or for $i^{\text{op}} = \sin^{-1}(\sqrt{2/5}) \approx 39.2^\circ$ (which is often called the "critical inclination" in the third-body perturbed problem). A solution of particular interest that is shown in Fig. 2 is the closed libration with

$$(e_o, i_o^{\text{op}}) = (0.6, 56.2^\circ) \text{ \& } \Omega^{\text{op}} = 0^\circ \rightarrow (e_o, i_o^{\text{op}}) = (0.6, 63^\circ) \quad (15)$$

with $\alpha = 0.198414$ and $\beta = -0.26098$. Using equation (12), the fixed point solution at $i_o^{\text{op}} = 56.2^\circ$ is found to have an eccentricity of $e \sim 0.7$. In Fig. 2 this value of eccentricity is at top of the loop formed by the solution in equation (15), and represents an upper bound to the largest value that this solution will have. The minimal value seen in the figure is the initial value of $e \sim 0.6$. The variation in inclination seen by this orbit can be ascertained from equation (13), and leads to $(i_{\text{min}}^{\text{op}}, i_{\text{max}}^{\text{op}}) = (51.4^\circ, 56.2^\circ)$. This range of values is useful for selecting a nominal semimajor axis value that satisfies the constellation coverage requirements and

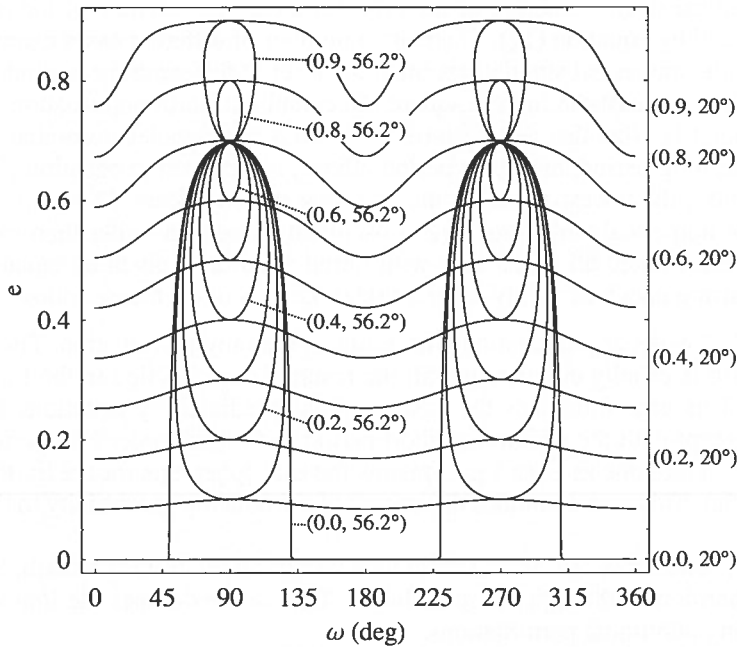


FIG. 2. Trajectories in the $e - \omega^{\text{op}}$ phase plane for selected initial values of eccentricity and inclination (e_0, i_0^{op}). All trajectories have initial arguments of perisaps $\omega^{\text{op}} = 90^\circ$ or 270° . In general, trajectories with initial inclinations above 39.6° will librate, and below will circulate.

has a sufficient perisaps altitude. First, to ensure perisaps altitudes are above a minimal altitude and apoapsis altitudes are less than a maximal altitude the constraints

$$a(1 - e_{\text{max}}) - R_M \geq h_{\text{min}} \quad \& \quad a(1 + e_{\text{max}}) - R_M \leq h_{\text{max}} \quad (16)$$

must be met where R_M is the mean radius of the Moon. A value for $h_{\text{min}} = 225$ km has been selected and leads to a semimajor axis value of $a \sim 6541.4$ km; and at apoapsis $h_{\text{max}} = 9382$ km. Coverage characteristics of this orbit are examined later in the constellation design step using numerical integrated trajectories being perturbed by a complete gravity model that includes the lunar nonspherical gravity, the Earth's gravity, and the Sun's gravity.

To summarize, the preceding development yielded an initial orbit selection with the initial values

$$\{a, e, i^{\text{op}}, \Omega^{\text{op}}, \omega^{\text{op}}\} = \{6541.4 \text{ km}, 0.6, 56.2^\circ, 0^\circ, 90^\circ\} \quad (17)$$

This selection has been made using the analytical solution given by equations (13) and (14) and results in a "frozen" orbit in $e - \omega^{\text{op}}$ phase space with an eccentricity variation of $\Delta e \sim +0.1$ and an inclination variation of $\Delta i^{\text{op}} \sim -4.8^\circ$. It is useful to examine the long-term stability of this orbit using a set of dynamical models of ever increasing fidelity.

Numerical Simulations of the Initial Orbit Design

These numerical investigation illustrate the impact of adding perturbations (i.e. adding nonspherical gravity effects and the Sun), changing to the IAU Moon Pole

frame, and the overall stability of the orbit for a ten-year lifetime of the reference orbit defined by equation (17). There are a number of different cases examined. In all cases, the numerical simulations integrate a set of differential equations that always include at least the inverse square effect and the Earth perturbation as given by equation (5). Note that the Earth perturbation is the complete term that includes all secular, long period, and short period effects, as opposed to equation (7) which only includes the lowest order secular and long period effects. The implication of this is the numerical simulations yield osculating elements rather than mean elements. Unless noted all orbits start with initial conditions given by equation (17) with a starting epoch of 1-July-2009 1:00:00. Details of each case follow:

1. *Case 1:* Two-year propagation with Earth as the only perturbation. The orbit of the Earth is exactly circular, and all the results are reconciled in the Earth orbit plane. This case illustrates the basic motions predicted by equations (13) and (14), except with the addition of short period and higher order Earth effects.
2. *Case 2:* The same as Case 1 except now the true ephemeris for the Earth is used (DE405s). This case examines the impact of introducing eccentricity to the Earth orbit.
3. *Case 3:* The same as Case 2 except now perturbations from the Earth, Sun, and zonal harmonics through J_7 are included. This case examines the impact of introducing additional perturbations.
4. *Case 4:* The same as Case 3 except now the frame has been switched to IAU Moon Pole. This examines the effect of switching from the Earth orbital plane to the Moon's equatorial plane.
5. *Case 5:* The same as Case 4 except now a complete 50×50 lunar gravity field is used. This case examines the effect of the additional zonals and tesseral harmonics on the evolution of the trajectory.
6. *Case 6:* The same as Case 4 except now the propagation interval is ten years. This case illustrates the long-term stability of the orbit and later will be used to demonstrate the coverage properties of the entire constellation.

Figure 3 shows the time histories of the *osculating* orbital eccentricity and inclination for Case 1. The first thing to note about the plots is the predominant long period (~ 1.25 years) oscillation with $\Delta e \sim 0.095$ and $\Delta i^{\text{op}} \sim 4^\circ$ which is indicative of the libration motion predicted by the mean element model. Also note the presence of a small amplitude ($\Delta e \sim 0.02$), faster eccentricity oscillation which indicates the

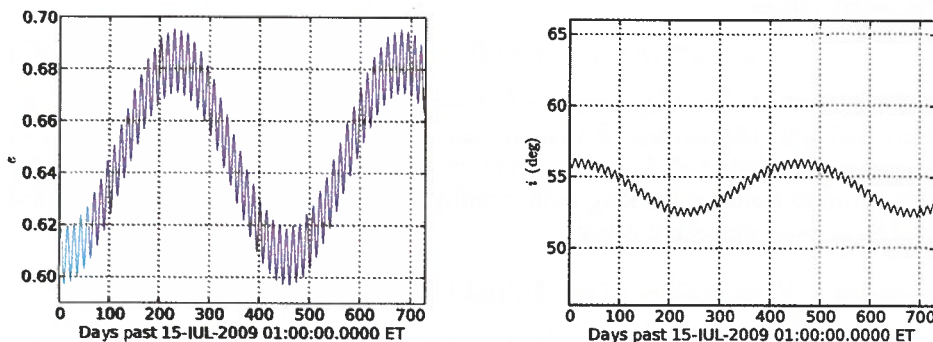


FIG. 3. Case 1 Eccentricity and Inclination Time Histories in the Earth Orbit Frame.

presence of the short periodic gravity effects that are not included in the mean element model. Indeed, the mean elements presented in Fig. 3 can be estimated to have initial values near $e_o \sim 0.61$ and $i_o^{op} \sim 55.9^\circ$ with mean value oscillations of $\Delta e \sim 0.07$ and $\Delta i^{op} \sim 3.4^\circ$. Using these values in equations (13) and (14) the predicted mean element variations are $\Delta e \sim 0.08$ and $\Delta i^{op} \sim 3.7^\circ$ which is a close match. The remaining differences are most likely attributable to the neglected higher order terms in the analytical model. These results validate the qualitative mean element model as a good representation of the numerical simulated model when only Earth gravity is present.

The next set of results examines the $e - \omega$ phase plane motion for the six cases. This reveals the overall stability of the libration motion under more realistic assumptions. The results are shown in Fig. 4. Examination of all cases shows that the

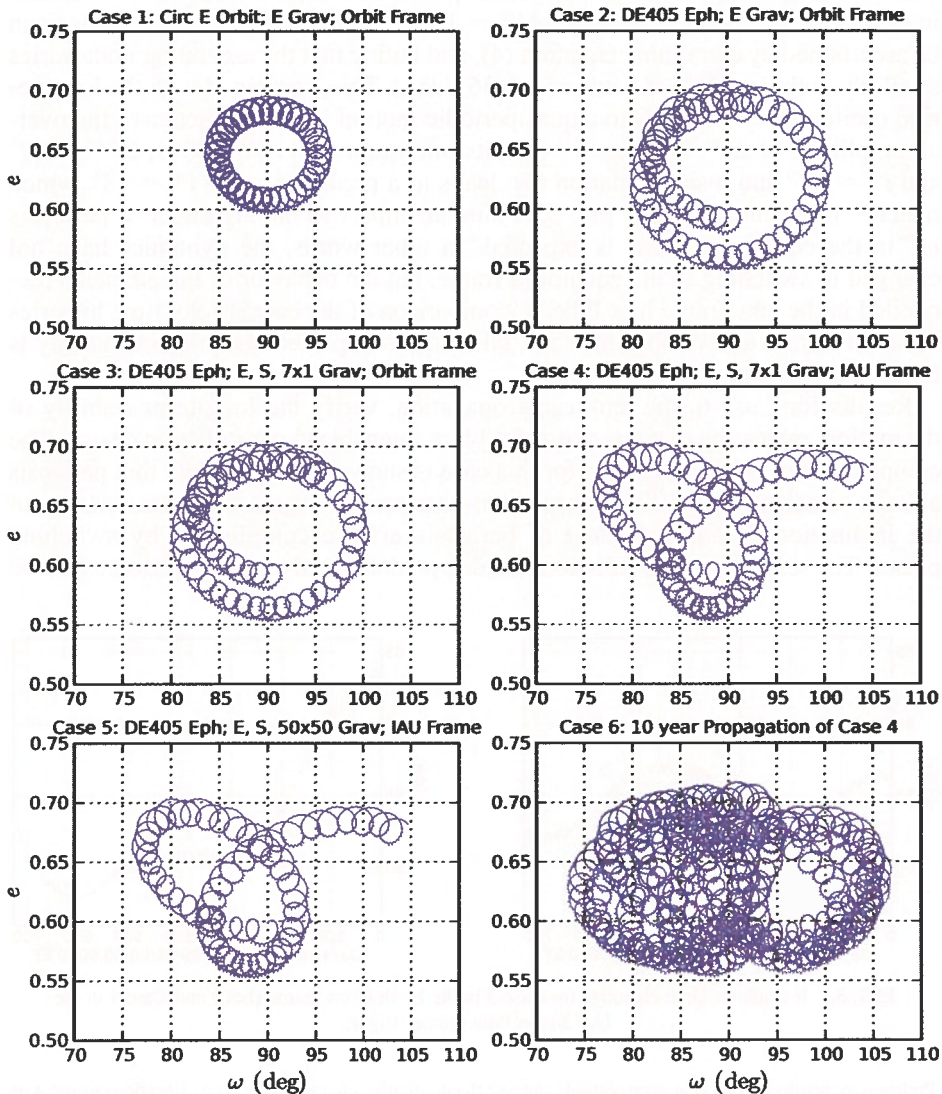


FIG. 4. $e - \omega$ Phase Plane Plots for the Six Cases.

$e - \omega$ libration motion is persistent, but significantly changes its characteristics in proceeding from Case 1 to 6. First note that the addition of the true ephemeris in Case 2 increases the size of the libration. For instance, the overall eccentricity variation grows to $\Delta e \sim 0.15$ from a value of 0.095 in Case 1. In Case 3 the addition of Sun gravity and zonal gravity in Case 3 do not significantly affect the motion over Case 2. In Cases 4, 5, and 6 the frame has changed to the IAU Moon Pole and the libration increases in complexity by adding some long period loops, however the motion is still bounded and the amplitude of the eccentricity variation remains about the same as in Cases 2 and 3 in the Earth orbit frame. It is worth noting that the addition of the complete 50×50 field had no significant impact on the overall results.

Better insight into what has happened to the solution in switching planes can be understood by examining the inclination time histories between Case 3 and Case 4. This is shown in Fig. 5 where the first thing to note is that in Case 3 $\Delta i^{\text{ep}} \sim 5^\circ$ and in Case 4 the variation increases to $\Delta i^{\text{ep}} \sim 15^\circ$. The explanation for this change can be ascertained by examining equation (4), and noting that the ascending node varies secularly with time Ω^{op} (at a rate of $-0.36^\circ/\text{day}$). This, combined with the long period oscillation of i^{op} , leads to a quasiperiodic motion in i^{ep} that increases the overall amplitude of Δi^{ep} . So when i^{ep} is at its minimum on 11-Apr-2011, $\Omega^{\text{op}} = 127^\circ$ and $i^{\text{op}} = 52^\circ$ and, using equation (4), leads to a predicted value $i^{\text{ep}} = 48^\circ$, which matches the value shown in Fig. 5. A similar impact to the argument of periapsis ω^{ep} in the equatorial frame is expected. In other words, the dynamics have not changed in switching to the equatorial frame, but the behavior of the elements reconciled in the new frame has. Indeed, comparison of the eccentricity time histories between frames shows no difference, which is as expected because eccentricity is frame independent.

Results for Case 6, the ten-year propagation, verify the long-term stability of the motion, indicating that this class of orbit is amenable to constellation design. The complete set of orbital elements for this case is shown in Fig. 6. Note that periapsis altitude remains above 100 km for the ten-year period.² Again the characteristics of the inclination i^{ep} and argument of periapsis ω^{ep} are complicated by switching planes. The semimajor axis variations are due predominantly to short periodic effects;

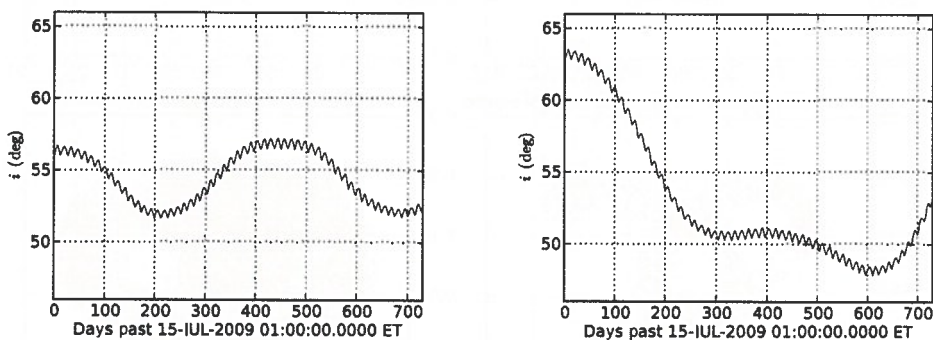


FIG. 5. Inclination Time Histories for Case 3 in the Earth Orbit Frame (Left) and Case 4 in the IAU Moon Pole Frame (Right).

²Preliminary results of 100 year propagations suggest the qualitative characteristics (i.e., libration) found with the ten-year propagations persist. A more detailed examination of longer period propagations is part of a future study.

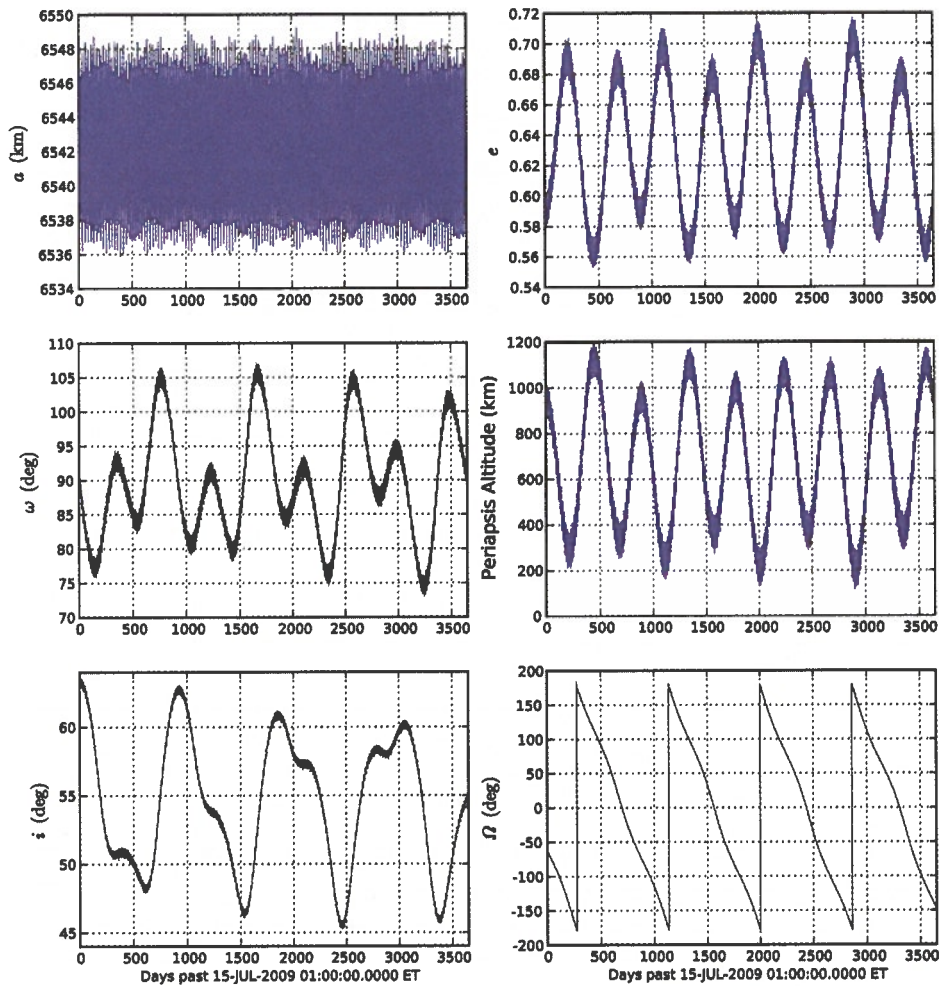


FIG. 6. Case 6 Orbital Element Time Histories in the IAU Moon Pole Frame.

any observed long period effects are minor. This indicates that the mean value of the semimajor axis is constant even in the presence of a complete gravity field. Since the mean motion n of the spacecraft is related to its semimajor axis value via $\sqrt{Gm_E/a^3}$ its average value is nearly constant, as well. Furthermore since the mean anomaly M is related to the mean motion n via $M = n(t - t_0)$, an average relative mean motion difference Δn between two spacecraft yields a secular variation in their relative mean anomalies (i.e., $\Delta M = \Delta n t$). The implication of this is that the average relative mean motion between spacecraft Δn can be *designed* to approach zero and the resulting average relative mean anomaly ΔM will be constant. This will turn out to be instrumental in designing a constellation with stable coverage properties.

Constellation Design for Polar Coverage

The design for the constellation will use the concept of an “eccentric street of coverage” (ESOC) as introduced by Ely, Crossley, and Williams [17] in which

satellites in the same plane equally spaced in initial mean anomaly are capable of providing focused coverage over a latitude range of interest. In the present study this latitude range is limited to a pole. To be specific the South Pole is selected for the remainder of the discussion. Before a detailed constellation design can begin, coverage by a single satellite to a South Pole station needs to be ascertained. In particular, the minimal coverage circle at apoapsis can be computed using the ten-year time history shown in Fig. 6. The relationship for the Moon central angle θ associated with the coverage circle has the relationship

$$\cos(\theta + \beta) = \frac{R_M}{R_M + h} \cos \beta = \frac{R_M \cos \beta}{a(1 - e^2)} (1 + e \cos f) \quad (18)$$

where β is the minimum elevation angle that a ground station can view the spacecraft, h is the spacecraft altitude, and f is spacecraft true anomaly. An illustration of the coverage circle geometry is shown in Fig. 7. For this study β is set to 10° . At an apoapsis of $f = 180^\circ$, equation (18) reduces to

$$\theta = \cos^{-1} \left[\frac{R_M \cos \beta}{a(1 + e)} \right] - \beta \quad (19)$$

For fixed β and a , equation (19) is minimized when e is smallest, which is ~ 0.55 . Using this value for e and a mean a of 6543 km leads to $\theta \sim 70^\circ$. Even at the largest inclination, this coverage circle lies over the South Pole (i.e., $\theta - (90^\circ - i^{sp}) > 0^\circ$). This verifies that over the ten-year mission a spacecraft in this orbit will see the South Pole during every orbital revolution.

Now to utilize the ESOC concept, a sufficient number of spacecraft must be placed in an orbital plane to provide continuous single and double fold coverage over the South Pole. Furthermore, because of the complex dynamics illustrated by the ten-year trajectory a central question is, "Does any design (ESOC or some other approach) yield stable coverage as the constellation evolves over time?" Because of the complexity of the motion it is nearly impossible to ascertain the coverage and stability of the design analytically, however, via numerical simulation, a design can be found that does provide stable two-fold coverage. The steps are as follows:

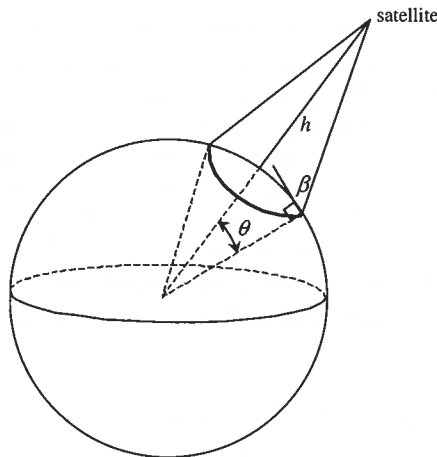


FIG. 7. Illustration of Coverage Circle Geometry.

1. Place n -spacecraft in the same initial orbits with initial mean anomaly separations of $360^\circ/n$. An initial selection for n can be made by analyzing coverage properties associated with the constellation using only Keplerian orbits.
2. Simulate the trajectories for a period of time that is sufficient to determine the average relative mean motion (and, by implication, the average relative semimajor axis differences) that are causing the spacecraft to drift apart in mean anomaly M . As indicated previously, this drift is essentially secular.
3. Estimate delta semimajor axis values for each spacecraft (other than the lead spacecraft) that will arrest the relative mean anomaly drift. That is, determine $\langle \Delta a_i \rangle \equiv \langle a_i - a_1 \rangle$ for each spacecraft $i \in (2, n)$ such that $\langle \Delta M_i \rangle = \langle M_i - M_1 \rangle$ are constants, where $\langle \cdot \rangle$ is an average operation.
4. Iterate Steps 2 and 3 until $\langle \Delta M_i \rangle$ is sufficiently constant.
5. Simulate the constellation with the adjusted values for a_i and calculate the coverage statistics to a polar station of interest. Reduce/increase the number of spacecraft to achieve the desired coverage (presently, this is two-fold coverage).

This design process is illustrated with the current orbit selection for South Pole coverage:

1. Three spacecraft are selected with the following initial conditions:

$$\begin{aligned} \{a_1, e_1, i_1^{\text{op}}, \Omega_1^{\text{op}}, \omega_1^{\text{op}}, M_1\} &= \{6541.4 \text{ km}, 0.6, 56.2^\circ, 0^\circ, 90^\circ, 0^\circ\}, \\ \{a_2, e_2, i_2^{\text{op}}, \Omega_2^{\text{op}}, \omega_2^{\text{op}}, M_2\} &= \{6541.4 \text{ km}, 0.6, 56.2^\circ, 0^\circ, 90^\circ, 120^\circ\}, \\ \{a_3, e_3, i_3^{\text{op}}, \Omega_3^{\text{op}}, \omega_3^{\text{op}}, M_3\} &= \{6541.4 \text{ km}, 0.6, 56.2^\circ, 0^\circ, 90^\circ, 240^\circ\} \end{aligned} \quad (20)$$

It can be shown that this constellation using only Keplerian orbits provides the desired one-fold and two-fold continuous coverage statistics.

2. These spacecraft trajectories are simulated for two years and the relative mean anomaly differences ΔM_2 and ΔM_3 are shown in Fig. 8. Note the secular change in the mean anomalies.
3. and 4. Iterating yields the adjustments to the semimajor axis values

$$\begin{aligned} a_2 &= \Delta a_2 + a_1 = 6541.623458 \text{ km} \\ a_3 &= \Delta a_3 + a_1 = 6539.069348 \text{ km} \end{aligned} \quad (21)$$

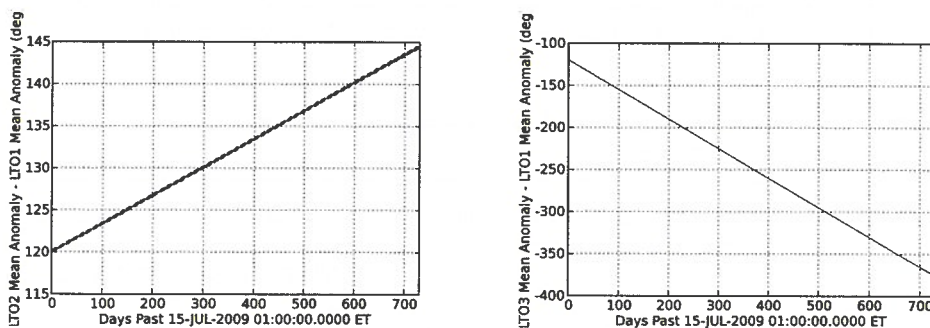


FIG. 8. Mean Anomaly Differences Between the Second Spacecraft (LTO2) and the First (LTO1), Left Figure, and the Third Spacecraft (LTO3) and the First, Right Figure, for the Constellation with No Phasing Adjustments.

No other adjustments to the elements are required. A two-year propagation of the relative mean anomaly differences ΔM_2 and ΔM_3 is shown in Fig. 9. Note that now the relative mean anomalies oscillate around a mean value that appears nearly constant. Hence, the spacecraft mean spacing is persistent in time with no additional orbit control required.

- Finally, the coverage statistics are computed using the constellation's ten-year propagated trajectories to a station located at the South Pole and a 10° minimum elevation angle with the results shown in Table 1. The rows include statistics for the mean pass, mean gap, and percent coverage. The columns include statistics for each satellite, and then one- and two-fold statistics for the entire constellation. The computation of the mean pass for the specified satellite is the average of its individual passes over the ten-year propagation period; the mean gap is the average period of time between passes for the specified satellite; and the percent coverage is the ratio of the sum of the passes over the entire period. Regarding the one- and two-fold constellation statistics, the one-fold mean pass is the average time that at least one satellite is in-view; and two-fold mean pass is the average time that at least two satellites are in-view. Similarly, the mean gap is the average time one or two satellites of the constellation are *not* in-view. Clearly, the constellation has the desired single and double fold coverage over the entire ten-year span. An example of the folds of coverage over the entire planet at the initial epoch is illustrated in Fig. 10, which clearly shows the two-fold coverage at the South Pole. The coverage at higher latitudes is very dynamic in time; hence general conclusions can not be drawn from this single snapshot. Additional analysis

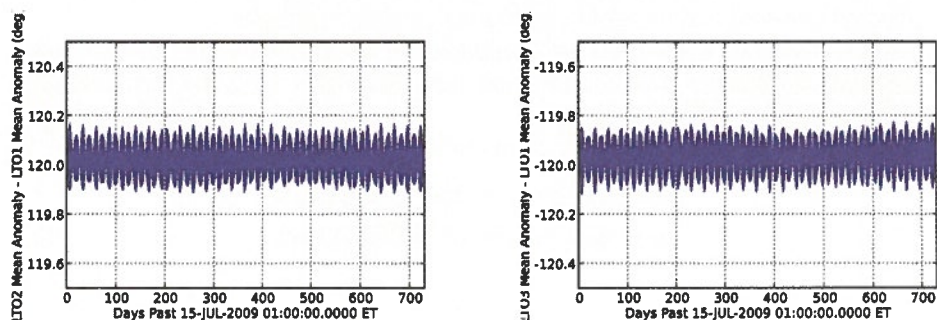


FIG. 9. Mean Anomaly Differences Between the Second Spacecraft (LTO2) and the First (LTO1), Left Figure, and the Third Spacecraft (LTO3) and the First, Right Figure, for the Phased Constellation.

TABLE 1. Coverage Statistics of a South Polar Station by each Spacecraft and the Constellation

	Satellite 1	Satellite 2	Satellite 3	Constellation	Constellation
				1-Fold Coverage	2-Fold Coverage
Mean Pass (hrs)	10.572	10.582	10.579	Total Span	Total Span
Mean Gap (hrs)	3.513	3.507	3.509	0	0
% Coverage	73.350	73.399	73.375	100	100

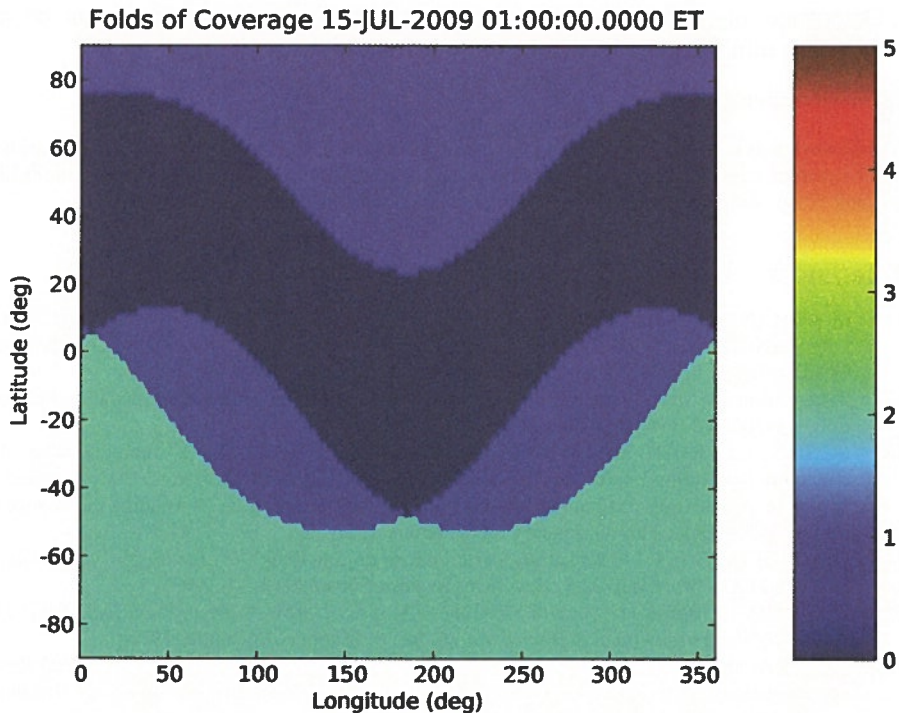


FIG. 10. Example illustrating the folds of coverage of the phased constellation for the initial epoch. The colorbar indicates the color associated with each integral fold of coverage.

has shown for the selected initial conditions that three spacecraft are the minimal number to achieve 100% two-fold coverage at the South Pole. Increasing the minimum elevation angle to 15° also reveals that this constellation still has 100% one-fold coverage, and 99.468% two-fold coverage.

Conclusion

A method has been developed for designing a high altitude lunar constellation that provides stable and redundant coverage to a selected pole at the Moon. The approach is guided by analytical techniques for initial orbit selection, and then a numerical procedure for tuning the coverage of the constellation to achieve a final design. The resulting constellation design yields stable orbits with lifetimes in excess of ten years, and a stable "formation." Under the influence of only gravity effects, the constellation requires no additional orbit control in order to maintain its formation. It is anticipated that a small amount of control will be required to accommodate other perturbations, such as solar radiation pressure, momentum desaturation errors, etc. Further work on the design methodology includes:

1. Analyze focused coverage at other latitude regions using the ESOC technique with this class of orbits.
2. Develop a semianalytical technique to establish the tuned initial semimajor axis values.
3. Analyze the effect of additional perturbations.
4. Conduct propagations for spans that are greater than ten years.

5. Determine any required formation maintenance approaches that might be required to minimize the impact of these perturbations.

Acknowledgments

This work was carried out at the Jet Propulsion Laboratory, California Institute of Technology, under contract with the National Aeronautics and Space Administration. The author would like to thank Gary Noreen for his initial insights into this constellation design problem.

References

- [1] FELDMAN, W. C., MAURICE, S., BINDER, A. B., BARRACLOUGH, B. L., ELPHIC, R. C., LAWRENCE, D. J. "Fluxes of Fast and Epithermal Neutrons from Lunar Prospector: Evidence of Water Ice at the Lunar Poles," *Science*, Vol. 281, September 4, 1998.
- [2] "The Vision for Space Exploration," National Aeronautics and Space Administration Publication, NP-2004-01-334-HQ, February 2004.
- [3] SCHIER, J. S., RUSH, J. R., WILLIAMS, W. D., VROTSOS, P. "Space Communications Architecture Supporting Exploration and Science: Plans and Studies for 2010–2030," presented as paper No. AIAA 2005-2517 at the 1st Space Exploration Conference: Continuing the Voyage of Discovery, Orlando, Florida, January 30–February 1, 2005.
- [4] GIACAGLIA, G. E. O. "Third Body Perturbations on Satellites," *Proceedings of the Artificial Satellite Theory Workshop*, U.S. Naval Observatory, November 8–9, 1993.
- [5] CUTTING, E., BORN, G. H., and FRAUTNICK, J. C. "Orbit Analysis for SEASAT-A," *The Journal of the Astronautical Sciences*, Vol. 26, No. 4, October–December 1978.
- [6] ELY, T. A. and HOWELL, K. C. "Dynamics of Artificial Satellite Orbits with Tesserel Resonances Including the Effects of Luni-Solar Perturbations," *International Journal of Dynamics and Stability of Systems*, Vol. 12, No. 4, December 1997.
- [7] KOZAI, Y. "Secular Perturbations of Asteroids with High Inclination and Eccentricity," *Astronomical Journal*, Vol. 67, No. 9, 1962.
- [8] LIDOV, M. L. "Evolution of Orbits of Artificial Satellites Affected by Third-Body Perturbations," *AIAA Journal*, Vol. 1, No. 8, 1963.
- [9] LORELL, J. "Long Term Behavior of Artificial Satellite Orbits Due to Third-Body Perturbations," *The Journal of the Astronautical Sciences*, Vol. 12, No. 4, Winter 1965.
- [10] BROUCKE, R. A. "Long-Term Third-Body Effects via Double Averaging," *Journal of Guidance, Control, and Dynamics*, Vol. 26, No. 1, January-February 2003.
- [11] PRADO, A. and FERNANDO, A. "Third-Body Perturbations in Orbits Around Natural Satellites," *Journal of Guidance, Control, and Dynamics*, Vol. 26, No. 1, January-February 2003.
- [12] SEIDELMANN, P. K., et. al. "Report of the IAU/IAG Working Group on Cartographic Coordinates and Rotational Elements of the Planets and Satellites: 2000," *Celestial Mechanics and Dynamical Astronomy*, Vol. 82, 2002.
- [13] URL to the planetary ephemeris files including the DE405 ephemeris file published by the Jet Propulsion Laboratory: http://ssd.jpl.nasa.gov/eph_info.html.
- [14] LIDOV, M. L. and YARSKAYA, M. V. "Integrable Cases in the Problem of the Evolution of a Satellite Orbit Under the Joint Effect of an Outside Body and of the Noncentrality of the Planetary Field," *Cosmic Research*, Vol. 12, No. 2, English Version Sept. 1974.
- [15] GOLDSTEIN, H. *Classical Mechanics*, second edition, Addison-Wesley, Reading, MA, 1980.
- [16] ELIPE, A. and LARA, M. "Frozen Orbits About the Moon," *Journal of Guidance, Control, and Dynamics*, Vol. 26, No. 2, March–April 2003.
- [17] ELY, T. A., CROSSLEY, W. A., WILLIAMS, E. A. "Satellite Constellation Design for Zonal Coverage Using Genetic Algorithms," *The Journal of the Astronautical Sciences*, Vol. 47, Nos. 3 and 4, July–December 1999.